THE JOURNAL OF PHYSICAL CHEMISTRY C

Article

Effect of BiVO4 Crystalline Phases on the Photoinduced Carriers Behavior and Photocatalytic Activity

Haimei Fan, Tengfei Jiang, Lingling Wang, Dejun Wang, Haiyan Li, Ping Wang, dongqing he, and Tengfeng Xie

J. Phys. Chem. C, **Just Accepted Manuscript** • DOI: 10.1021/jp206798d • Publication Date (Web): 04 Nov 2011

Effect of $BiVO_4$ Crystalline Phases on the photoinduced carriers behavior and photocatalytic activity

Haimei Fan[a], Tengfei Jiang[a], Lingling Wang[a c], Dejun Wang[a], Haiyan Li[a], Ping Wang[b], Dongqing He[a] and Tengfeng Xie[a]*

[a] State Key Laboratory of Theoretical and Computational Chemistry, College of Chemistry, Jilin University, Changchun 130012, China

[b] State Key Laboratory of Electroanalytical Chemistry, Changchun Institute of Applied Chemistry, Chinese Academy of Sciences, Changchun 130022, China

[c] State Key Laboratory of Supramolecular Structure and Materials College of Chemistry, Jilin University, Changchun, 130012, China

E-mail: **xietf@jlu.edu.cn**

* Corresponding author. Fax: (+86) 431-8516-8093. E-mail: xietf@jlu.edu.cn

Abstract: A series of different crystalline phases $BiVO_4$ photocatalysts (tetragonal, monoclinic and monoclinic/tetragonal heterophase) have been prepared by a coprecipitation and molten salt method. High resolution transmission electron microscopy (HRTEM) results show that an interface of intimate contact is formed in monoclinic/tetragonal heterophase and monoclinic phase is mainly on the surface of nanoparticles. Surface photovoltage (SPV) and transient photovoltage (TPV) technique are used to further investigate the transfer process of photoinduced charge carriers. The results show that the behavior of photoinduced charges markedly depend on the crystalline phases of $BiVO_4$ samples and the presence of interface in monoclinic/tetragonal heterophase provides a spatial condition for charge transfer, promotes the separation of photoinduced electron–hole pairs and changes the migration direction of photoinduced carriers. The relationship between behavior of photoinduced charge carriers and photocatalytic activity was discussed in detail, which would provide a greater insight into the intrinsic reasons of the enhancement in photocatalytic activity.

Keywords: crystalline phases, photoinduced carriers, photocatalytic activity, interface

Introduction

As an ideal green technology, semiconductor photocatalyst has attracted continuous interest for its potential applications in environmental cleaning and solar energy utilization.[1–3] Bismuth vanadate ($BiVO_4$), one of the most promising semiconductors for its various potential applications for solar energy conversion and storage, [4–6] has been devoted to considerable research efforts. It is well known that $BiVO_4$ mainly exists in three crystalline phases: tetragonal zircon (z–t), monoclinic scheelite (s–m) and tetragonal scheelite structure (s–t).[7] The process of phase transformation among them has been studied. When tetragonal zircon $BiVO_4$ is heated up to 400–500 ℃, monoclinic scheelite $BiVO_4$ is obtained, conversely, the phase transformation between monoclinic scheelite $BiVO_4$ and tetragonal scheelite $BiVO_4$ occurs reversibly at 255 ℃.[8] Zhang et al. selectively synthesized $BiVO_4$ with different crystalline phases and found that monoclinic $BiVO_4$ with a band gap of 2.34 eV showed higher photocatalytic activity than that of tetragonal $BiVO_4$.[9] Feng and co-workers prepared $BiVO_4$ nanoparticles by molten salt method. And the shift of Raman peak position indicates that the symmetry distortions in the local structure of the monoclinic $BiVO_4$. The variations of the local structure result in the modification of the electronic structure, which is responsible for the high visible-light photocatalytic activity.[10] Akihiko Kudo and coworkers considered that thedistortion of a Bi–O polyhedron by a $6s^2$ lone pair of Bi^{3+} may play an important role in improving the photocatalytic activity of monoclinic $BiVO_4$ under visible light irradiation. The distortion probably affects the charge separation and delocalization of photogenerated electrons and holes.[11] These reports indicate that the photocatlytic performance of $BiVO_4$ largely depends on the crystalline phases and the behavior of photoinduced charge carriers. Therefore, a better understanding about the relationship of the change of crystalline phase and transfer of photoinduced charge carriers would provide greater insight into the substaintial reasons of the enhancement of photocatalytic activity. Up to now, many research teams have reported the preparation of $BiVO_4$ with different morphologies and crystalline phases, however, the transfer character of photoinduced charge carries in different crystalline phase and the interfacial influence on photoinduced charge behavior in heterophase are still ambiguous, no such work has been reported up to

date. Therefore, techniques which can directly detect the surface electronic potentials and the behavior of photoinduced charge carriers are desirable.

The surface photovoltage (SPV) technique based on lock-in amplifier, as a well-established contactless and nondestructive technique, especially combined with the transient photovoltage (TPV) measurement could directly provide information about separation, transportation and recombination of photoinduced charge carriers. It is a rapid and effective method to study the photovoltaic properties of semiconductor photocatalysts.[12−15]

Herein, we prepared and well characterized different crystalline phase $BiVO_4$ (tetragonal, monoclinic and tetragonal/monoclinic heterophase) photocatalysts. An effectively interfacial electric field was formed in tetragonal/monoclinic heterophase $BiVO_4$ and monoclinic scheelite $BiVO_4$ was mainly on the surface of nanoparticles. The SPV and TPV technique were used to study the behavior (including separation, transport and recombination) of photoinduced charge carriers in different crystalline phase $BiVO_4$, and the relationship between photocatalytic activity and behavior of photoinduced charge carriers was discussed detailedly.

Experimental section

Preparation of $BiVO_4$. $BiVO_4$ (z−t) was prepared by the coprecipitation method.[10] NH_4VO_3 and $Bi(NO_3)_3{\cdot}5H_2O$ of analytic reagent grade were used as starting materials. A typical procedure as follows: 1.17 g NH_4VO_3 and 4.85 g Bi $(NO_3)_3{\cdot}5H_2O$ were added into 200 mL distilled water under stirring, and a yellow precipitate was formed. The precipitate was filtered, and washed with distilled water, dried at 100 ºC for 5 h, and referred to as-prepared $BiVO_4$ ($BiVO_4$−A). The as-prepared $BiVO_4$−A was mixed with $LiNO_3$ salt by ultrasonic at room temperature (with initial $LiNO_3$: $BiVO_4$ molar ratio of 12:1). The mixture was heated at 270 ºC for 6 h. Then, $LiNO_3$ was removed from the product by washing with distilled water. The prepared product was referred as $BiVO_4$−B. Directly heating the as-prepared $BiVO_4$–A at 500 ºC for 4 h, the product was referred as $BiVO_4$−C.

Photocatalytic Test. Photocatalytic activities of samples were determined by the degradation of Methylene Blue (MB) aqueous solution under visible light ($\lambda > 400$ nm) and UV light irradiation in a

home-made quartz photochemical reactor. A 500 W Xenon lamp (CHFXQ500 W) with a 400 nm UV cut off filter was used to as the light source. A high-pressure mercury lamp (500 W) was used as the UV light source. Experiments were performed at ambient temperature as follows: 0.020 g photocatalyst was added to 20 ml MB (10 mg/L) aqueous solution. Before irradiation, the mixture was first sonicated for 5 min and then kept in the dark for 1 h to reach the adsorption–desorption equilibrium under magnetically stirring. At the same irradiation time intervals, analytical samples were taken from the suspension and immediately centrifuged at 10,000 rpm for 5 min, the concentration analysis of MB was determined by using an Ocean Optics Miniature Fiber Optic Spectrometer (Maya 2000 Pro).

Characterization. The crystalline phases were identified by X-ray diffraction (XRD) using a Rigaku D/Max-2550 diffractometer with Cu Kα radiation (λ = 1.5418 Å) at 50 kV and 200 mA in the range of 10–70° (2θ) at a scanning rate of 10° min^{-1}. The UV–vis diffuse reflectance spectra were recorded with a Shimadzu 3600 UV–vis–NIR spectrophotometer equipped with an integrating sphere diffuse reflectance accessory, while $BaSO_4$ was used as a reference.

The surface photovoltage (SPV) measurement system included a source of monochromatic light, a lock-in amplifier (SR830-DSP) with a light chopper (SR540), a photovoltaic cell, and a computer. A 500 W xenon lamp (CHFXQ500 W, Global Xenon Lamp Power) and a double-prism monochromator (Zolix SBP500) provided monochromatic light as the source light. The samples were studied without further treatment during the SPV measurement, and the contact between samples and the indium tin oxide (ITO) electrode was not ohmic when we carried out the measurement of surface photovoltage. The construction of the photovoltaic cell is a sandwich-like structure of ITO–sample–ITO. We put the powder sample on the ITO electrode and press it with another ITO electrode to obtain a film composed of the powder sample.

TPV measurement was carried out in a device which was described in our previous work.[12–14] A parallel-plate capacitor like sample chamber consisted of the $BiVO_4$ electrode, a piece of 10 μm thick mica and a platinum wire gauze electrode. A laser radiation pulse (wavelength of 355 nm and pulse

width of 5 ns) from a third-harmonic Nd:YAG laser (Polaris II, New Wave Research, Inc.) was used to excite the TPV. The signals were registered by a 500 MHz digital phosphor oscilloscope (TDS 5054, Tektronix) with a preamplifier. The formation of a TPV signal was determined by the factors of light absorption, transport of excess carriers, structural and electric characteristics of a semiconducting material. Both the TPV and SPV measurements were performed in air atmosphere at room temperature.

Results and Discussion

Figure 1 shows the XRD patterns of $BiVO_4$–A, $BiVO_4$–B and $BiVO_4$–C. $BiVO_4$–A can be well indexed to be tetragonal zircon (z-t) structure with the present of peaks $2\theta = 24.4°$, 32.7° (JCPDS No. 14-0133) and $BiVO_4$–C to be monoclinic scheelite (s-m) structure with the peaks of $2\theta = 28.8°$ (JCPDS No. 14-0688).[11] While $BiVO_4$–B is a heterophase including tetragonal zircon and monoclinic scheelite. According to $V_{Monoclinic} = I_{Monoclinic\ (121)} / (I_{Monoclinic\ (121)} + I_{Tetragonal\ (200)})$ from XRD patterns,[16] $BiVO_4$ (s–m) percentage is 25.34 % in the heterophase.

Figure 2 displays the UV–vis diffuse reflectance spectra of the as-prepared samples. As can be seen from Figure 2, the absorption edges of $BiVO_4$ samples somehow varied in an orderly fashion. Different phases of $BiVO_4$ powders result in different band gaps. With the phase transition from tetragonal to monoclinic phase, the band gaps tend to red shift. And these clearly demonstrate that the electronic structures of $BiVO_4$ are also changed with the phase transition process.[17]

High-resolution transmission electron microscopy (HRTEM) was used to characterize the microstructure of $BiVO_4$–B, which were shown in Figure 3. The image in Figure 3 (a) demonstrates that the $BiVO_4$ particles prepared under our procedure are nano-particles with diameters in a range of 10 to 40 nm. The lattice spacing of 0.226 nm in Figure 3 (b) corresponds to the (211) crystalline plane of monoclinic scheelite (s-m) $BiVO_4$, whereas the fringe of 0.299 nm matches the (101) crystallographic planes of tetragonal zircon (z–t) $BiVO_4$, which are good accordance with the results of the XRD patterns (Figure 1). This clearly indicates that a tight interface junction has been formed between $BiVO_4$ (s–m) and $BiVO_4$ (z–t) in a nano-size level.

The SPV measurement is used to investigate the transfer behaviour of potoinduced charge carries with high sensitivity to defect states in the sample at its surface, bulk, or any buried interface. It is well known that a photovoltage arises whenever photoinduced charge carriers are separated in space. Therefore, the formation of a SPV signal is determined by the fundamental properties of the light absorption and the transport of excess carriers in a semiconducting material.[18-22] The preview reports indicate that a negative SPV signal means that photoinduced electrons transfer to the irradiation side of the sample, and a positive SPV signal suggests photoinduced holes move to the irradiation side of the sample.[23]

Figure 4 shows the SPS signal of samples $BiVO_4$–A, $BiVO_4$–B and $BiVO_4$–C. The response of $BiVO_4$–A shows a negative SPV signal in the range of 300–410 nm, which means the photoinduced electrons move to the surface of the sample, and photoinduced holes migrate from the surface to the bulk. Whereas, the response of $BiVO_4$–C shows a positive signal in the range of 300–510 nm which means the photoinduced electrons migrate from the surface to the bulk, and photoinduced holes move to the surface. The band gap of $BiVO_4$–A and $BiVO_4$–C were about 2.9 eV and 2.4 eV, respectively, by calculation from the SPS data ($E = 1240/\lambda$), which is consistent with the previous report.[24]

Interestingly, for the $BiVO_4$–B a negative signal in the visible light region (400–510 nm) and a positive signal in the UV region (300–400 nm) were obtained, respectively. According to the result, we considered that the possible reasons of SPV inversion between 300 nm and 500 nm as follows: the absorption coefficient of $BiVO_4$ is different with the vary of incident wavelength, in general, the absorption coefficient is smaller for visible light and larger for UV light. Therefore, the light penetrating depth of different wavelengths is different. Generally, penetrating depth of incident light decreases with the increasing of incident wavelength. Under the UV light irradiation (300–400 nm), the transmission depth is very small, only the surface of $BiVO_4$ (s–m) could be excited, photoinduced charge carriers are separated under the effect of built-in electric field in the surface space charge region. Photoinduced holes move to the surface and accumulated nearby, and a positive response signal appeared in the SPS curve. While, for the visible light region (400–500 nm), the penetrating depth of incident light is deeper,

and that could reach the interface of heterophase. The photoinduced charge carriers generated both at the surface and bulk of heterophase $BiVO_4$ nanoparticles, and separated under the effect of surface electric field and interface electric field simultaneously. We speculate that an interfacial electric field are formed on the contact interface due to the different of band gap and band position between $BiVO_4$ (s–m) and $BiVO_4$ (z–t), and the direction of interface electric field is from $BiVO_4$ (s–m) to $BiVO_4$ (z–t). A negative signal means photoinduced electrons accumulate at the surface which indicates that the interface electric field dominants the charge separation.

In order to compare the effect of interfacial electric field in $BiVO_4$–B, we directly mix $BiVO_4$–A and $BiVO_4$–C with the same proportion of $BiVO_4$–B (the percentage of $BiVO_4$–C is 25.34%),[25] and the SPS is shown in Figure 5. There is a positive SPV response band in the range of 410–510 nm corresponding to the response of $BiVO_4$–C and a positive response in 300–410 nm which consistent with the response of $BiVO_4$–A, respectively. The response of mixture is a simply add with the response of $BiVO_4$–A and $BiVO_4$–C. This result gives us an indirect evidence for the existence of effective interface in $BiVO_4$–B. However, the detail properties of the interfacial electric field are not yet clear and still need further studied.

The TPV measurements were carried out to investigate the kinetics property of the photoinduced charge carriers in our system. It provides direct information about the generation, separation, and recombination of photogenerated charge carriers. Figure 6 shows the TPV response of difference crystalline phase $BiVO_4$ under wavelengths of 355 nm, when the intensity of the laser pulse (excitation level) was 50 μJ. According to the TPV results, the following features can be found: (1) All the samples have a strong TPV response under the irradiation of UV light indicating a high efficiency of charge separation. (2) The TPV response signal of $BiVO_4$–A is negative, but that of $BiVO_4$–B and $BiVO_4$–C are positive. (3) Three peaks can be observed that there are two response components and the TPV maximums (t_{max}) are 3×10^{-7}s for $BiVO_4$-A, 1×10^{-5}s for $BiVO_4$-B and 2×10^{-4}s for $BiVO_4$-C, respectively.

It is well known that a photovoltage arises whenever light-induced excess charge carriers are separated in space.Therefore, the formation of a TPV signal is determined by the fundamental properties

of the light absorption and the transport of excess carriers in a semiconducting material or device. According to our previous report, a positive TPV response implies that negative charges transfer toward the bulk, positive charges transfer to the surface and accumulate at the surface area nearby.[12–14] Therefore, for the $BiVO_4$–A sample, a negative signal implies that photoinduced electrons move to the surface and accumulate under nearby, photoinduced holes transfer to the bulk. On the contrary, for $BiVO_4$–B and $BiVO_4$–C, the positive signal implies that photoinduced electrons move to the bulk of sample, photoinduced holes transfer toward the surface of samples and accumulated under nearby. This result is consistent with the discussion of SPS. Besides, the time of the maximums (t_{max}) of the TPV can give information about the recombination time of photoinduced charge carriers[26]. As shown in figure 6, the order of t_{max} is $BiVO_4$-C > $BiVO_4$-B >$BiVO_4$-A, that is, the recombination of charge carriers in $BiVO_4$ (s–m) and heterophase is much slower than in $BiVO_4$ (z–t), which is beneficial to improve the photocatalytic ability of samples.

In order to further investigate the behaviour of photoinduced charge carriers, we also show the TPV curve of direct mixture in Figure 7. The direct mixture has a negative TPV response indicating photoinduced electrons transfer to the surface of sample and photoinduced holes toward the bulk, which is similar with the response of $BiVO_4$–A. This may indicate that there is no interaction between $BiVO_4$–A and $BiVO_4$–C for direct mixture.

Photocatalytic activity of samples

The photocatalytic activity of $BiVO_4$ samples was evaluated by the degradation of MB in aqueous solution under visible light and UV light irradiation. The results were shown in Figure 8 and Figure 9. Under the irradiation of visible light (λ>400 nm), the decomposition of MB dye over $BiVO_4$–C sample is up to about 70% after 150 min which is much higher than that of $BiVO_4$–A (10%) and $BiVO_4$–B (15%). However, under the irradiation of UV light, the photocatalytic efficiency of $BiVO_4$–C and $BiVO_4$–B was similar about 50% and 48% after 150 min, respectively, which is much higher than that of $BiVO_4$–A (almost has no photocatalytic activity). Reaction constants are 0.00363 min^{-1}, 0.00079 min^{-1}, and 0.00047 min^{-1}under the irradiation of visible light, and the reaction constants are 0.00212 min^{-1},

0.00027 min^{-1} and 0.00023 min^{-1} under the irradiation of UV light for $BiVO_4$-C, $BiVO_4$-B, and $BiVO_4$-A. Comparing the reaction constant, the degradation rates of MB showed large differences for $BiVO_4$ with different phases. And the $BiVO_4$-C has the higher photocatalytic activity.

In order to demonstrate the significance of effective interface in $BiVO_4$–B for photocatalytic activity, the direct mixture is used as a reference. Under visible light, its activity is similar to $BiVO_4$–C and under the UV light irradiation is similar to $BiVO_4$–A (in Figure 8 and Figure 9), and the reaction constant is 0.00172 min^{-1} and 0.00201 min^{-1}, indicating the mixed sample is only a two phases composition and no effective interface is formed between them.

Photocatalytic activity is influenced by many factors in which specific surface area and the transport properties of photoinduced charge carriers are two key factors. The surface area values are 4.85 m^2/g, 0.97 m^2/g and 1.61 m^2/g for $BiVO_4$–A, $BiVO_4$–B, $BiVO_4$–C, respectively. Obviously, their surface areas are relatively low which indicates that the surface area is not the major reason for the different photocatalytic activity. Thus, the photoinduced charge carriers transport properties in the semiconductor must play an important role in improving the photocatalytic activity. For $BiVO_4$ system, photooxidations occurring in aqueous media, the mechanism may involve direct reaction of the organic chemical (dye) with surface h_{vb}^+, indirect reaction with OH· radicals, or a dual mechanism involving both surfacce h_{vb}^+ and OH· radicals.[26, 27] The pathway of photocatalytic degradation can be described through out the following equations:

$$2\ BiVO_4 + h\nu \rightarrow\ BiVO_4\ (h_{vb}^+) + BiVO_4\ (e^-)$$

$$H_2O + BiVO_4\ (h_{vb}^+) \rightarrow OH\cdot + H^+ + BiVO_4$$

$$h_{vb}^+/OH\cdot + MB \rightarrow \text{products}$$

In view of these results, the transfer properties of photoinduced charge carriers have an important effect on its photocatalytic activity. For the oxidation process of photoinduced holes photocatalysis mechanism of $BiVO_4$, the more photoinduced holes accumulated on the surface of $BiVO_4$ nanoparticles,

the higher photocatalysis efficiency it has. Compared with the SPV and TPV results, we could understand the result of photocatalytic activity.

For $BiVO_4$–A, photoinduced electrons accumulated nearby the surface, there is nearly no photoinduced holes to oxidize dye or form OH· radicals, so it has almost no photocatalytic activity under the irradiation of either visible light or UV light. While for $BiVO_4$–C, photoinduced holes transfer to the surface and accumulated on it with the irradiation either visible or UV light. Therefore, $BiVO_4$–C has much higher photocatalytic activity. However, for the $BiVO_4$–B sample, there are two response processes in the curve of SPV. First, photoinduced holes transfer toward the surface and accumulated nearby under the UV light irradiation which is of benefit to the photocatlysis. Second, under the irradiation of visible light, photoinduced electrons accumulate nearby the surface. So $BiVO_4$–B has higher photocatalytic activity under the irradiation of UV light.

Conclusion

In tetragonal/monoclinic heterophase $BiVO_4$, a tight interface junction has been formed between $BiVO_4$ (s–m) and $BiVO_4$ (z–t) in a nano-size level. Monoclinic scheelite $BiVO_4$ (s-m) was mainly at the surface region of heterophase $BiVO_4$ nanoparticles after calcination. The SPS and TPV results indicate that the transfer directions of photoinduced charge carriers are different in $BiVO_4$ (s–m) and $BiVO_4$ (z–t). Under visible light irradiation photoinduced holes accumulate at the surface of monoclinic $BiVO_4$ (s-m), which is corresponding to the highest photocatalysis efficiency because of the oxidation mechanism of photoinduced holes for $BiVO_4$ photocatalyst. This work is anticipated to open a new possibility in the investigation of $BiVO_4$ with different crystalline phases and promotes their practical application in addressing various environmental issues.

Acknowledgment

We are grateful to the National Basic Research Program of China (973 Program) (2007CB613303), the National Natural Science Foundation of China (21173103, 51172090) and the Science and Technology Developing Funding of Jilin Province (201115012) for the financial support.

References

(1) Radim B.; Bernhard N.; Shanmugasundaram S.; Marcin J.; Thomas D.; Helmut T.; Horst K. Chemical Physics. 2007, 339, 11.

(2) Zhong, Z. Y.; Judith H.; Jaclyn T.; Shen, S. C.; Aharon G. Chem. Mater. 2007, 19, 4776.

(3) Sachiko T.; Takashi T.; Mamoru F.; Tetsuro M. J. Phys. Chem. C. 2008, 112, 14948.

(4) Li, M. T.; Zhao, L.; Guo, L. J. international journal of hydrogen energy. 2010, 35, 7127.

(5) Zhao, Y.; Xie, Y.; Zhu, X.; Yan, S.; Wang, S. X. Chem. Eur. J. 2008, 14, 1601.

(6) Yin, W. Z.; Wang, W. Z.; Shang. M.; Zhou, L.; Sun, S. M.; Wang, L. Eur. J. Inorg. Chem. 2009, 4379.

(7) Lim, A. R.; Choh, S. H.; Jang, M. S. J. Phys: Condens. Matter. 1995, 7, 7309.

(8) Bierlein, J. D., Sleight, A. W. Solid State Commun. 1975, 16, 69.

(9) Zhang, X.; Ai, Z. H.; Jia, F. L.; Zhang, L. Z.; Fan, X. X.; Zou, Z. G. Materials Chemistry and Physics. 2007, 103, 162.

(10) Li, Ch. G.; Pang, G. Sh.; Sun, Sh. M.; Feng, S. H. J Nanopart Res 2010, 12, 3069.

(11) Saimi T.; Hideki K.; Akihiko K. Chem. Mater. 2001, 13, 4624.

(12) Zhang, Y.; Xie, T. F.; Jiang, T. F.; Wei, X.; Pang, S.; Wang, X.; Wang, D. J., Nanotechnology 2009, 20, 155707.

(13) Wei, X.; Xie, T. F.; Xu, D.; Zhao, Q. D.; Pang, S.; Wang, D. J. Nanotechnology 2008, 19, 275707.

(14) Zhang, Q. L.; Wang, D. J.; Wei, X.; Xie, T. F.; Li, Z. H.; Lin, Y. H.; Yang, M. Thin Solid Films 2005, 491, 242.

(15) Jiang, T. F.; Xie, T. F.; Zhang, Y.; Chen, L. P.; Peng, L. L.; Li, H. Y.; Wang, D. J. Phys. Chem. Chem. Phys. 2010, 12, 15476.

(16) Ke, D. N.; Peng, T. Y.; Ma, L.; Cai, P.; Dai, K. Inorg. Chem. 2009, 48, 4685.

(17) Zhang, H. M.; Liu, J. B.; Wang, H.; Zhang, W. X.; Yan, H. J Nanopart Res, 2008, 10, 767.

(18) L. Kronik; Y. Shapira. Surface Science Reports, 1999, 37, 1.

(19) Xie, T. F.; Wang, D. J.; Zhu, L. J.; Wang, C.; Li, T.J.; Zhou, X. Q.; Wang, M. J. Phys. Chem. B, 2000, 104, 8177.

(20) Gross, D.; Iván Mora-Seró, Thomas Dittrich, Abdelhak Belaidi, Christian Mauser, Arjan J. Houtepen, Enrico Da Como,Andrey L. Rogach, Jochen Feldmann. J. Am. Chem. Soc., 2010, 132, 5981.

(21) F. Andrew Frame, Troy K. Townsend, Rachel L. Chamousis, Erwin M. Sabio, Th. Dittrich, Nigel D. Browning, Frank E. Osterloh. J. Am. Chem. Soc. 2011, 133, 7264.

(22) Zhang, J.; Wang, D. J.; Shi, T. Sh.; Wang, B. H.; Sun, J. Z.; Li, T. J. Thin Solid Films, 1996, 284, 596.

(23) V, Duzhko. ; V, Yu. Timoshenko. ; F. Koch. ; Th. Dittrich. PHYSICAL REVIEW B, 2001, 64 075204-1.

(24) Akihiko, K.; Keiko, O.; Hideki, K. J. Am. Chem. Soc. 1999, 121, 11459.

(25) Lin, X. P.; Xing, J. C.; Wang, W. D.; Shan, Z. C.; Xu, F. F.; Huang, F. Q. J. Phys. Chem. C. 2007, 49, 18288.

(26) Li, H. Y.; Wang, D. J.; Fan, H. M.; Wang, P.; Jiang, T. F.; Xie, T. F. Journal of Colloid and Interface Science. 2011, 354, 175.

(27) Shi, R.; Huang, G. L.; Lin, J.; Zhu, Y. F. J. Phys. Chem. C. 2009, 113, 19633.

(28) A. Martínez-de, L. C.; U.M. GarcíaPérez. Materials Research Bulletin. 2010, 45, 13

Figure Captions

Figure 1. The XRD patterns of $BiVO_4$–A, $BiVO_4$–B and $BiVO_4$–C.

Figure 2. UV–vis absorption of $BiVO_4$–A, $BiVO_4$–B and $BiVO_4$–C.

Figure 3. HRTEM image of $BiVO_4$–B, the inset in (b) shows the corresponding Fast Fourier transform (FFT) patterns.

Figure 4. The surface photovoltage spectra (SPS) of samples: $BiVO_4$–A, $BiVO_4$–B and $BiVO_4$–C. Inset is schematic diagram of SPV measurement.

Figure 5. The SPS of direct mixture with the $BiVO_4$–C/$BiVO_4$–A mass ratio of 25.34 %.

Figure 6. The transient photovoltage (TPV) responses of $BiVO_4$. The wavelength and intensity of excitation pulse are 355 nm and 50 μJ, respectively.

Figure 7. TPV curve of direct mixture with the $BiVO_4$–C/$BiVO_4$–A mass ratio of 25.34 %. The wavelength and intensity of excitation pulse are 355 nm and 50 μJ, respectively.

Figure 8. Kinetics of photodegradation of MB using $BiVO_4$ with different crystalline phases under the irradiation of visible light ($\lambda > 400$ nm $C_{MB} = 10$ mg/L).

Figure 9. Kinetics of photodegradation of MB using $BiVO_4$ with different crystalline phases under the irradiation of UV light ($C_{MB} = 10$ mg/L).

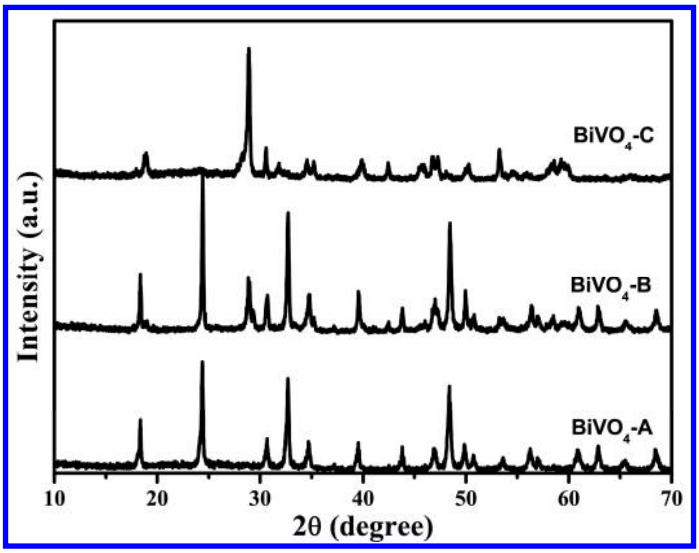

Figure 1. The XRD patterns of $BiVO_4$–A, $BiVO_4$–B and $BiVO_4$–C.

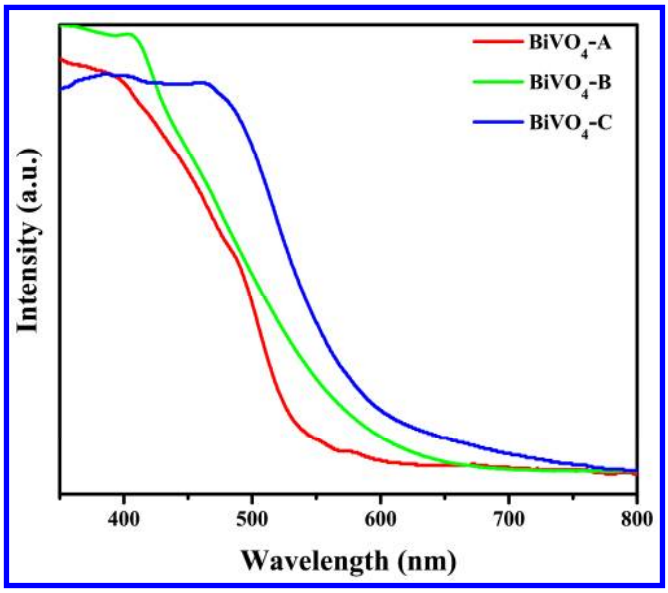

Figure 2. UV–vis absorption of $BiVO_4$–A, $BiVO_4$–B and $BiVO_4$–C.

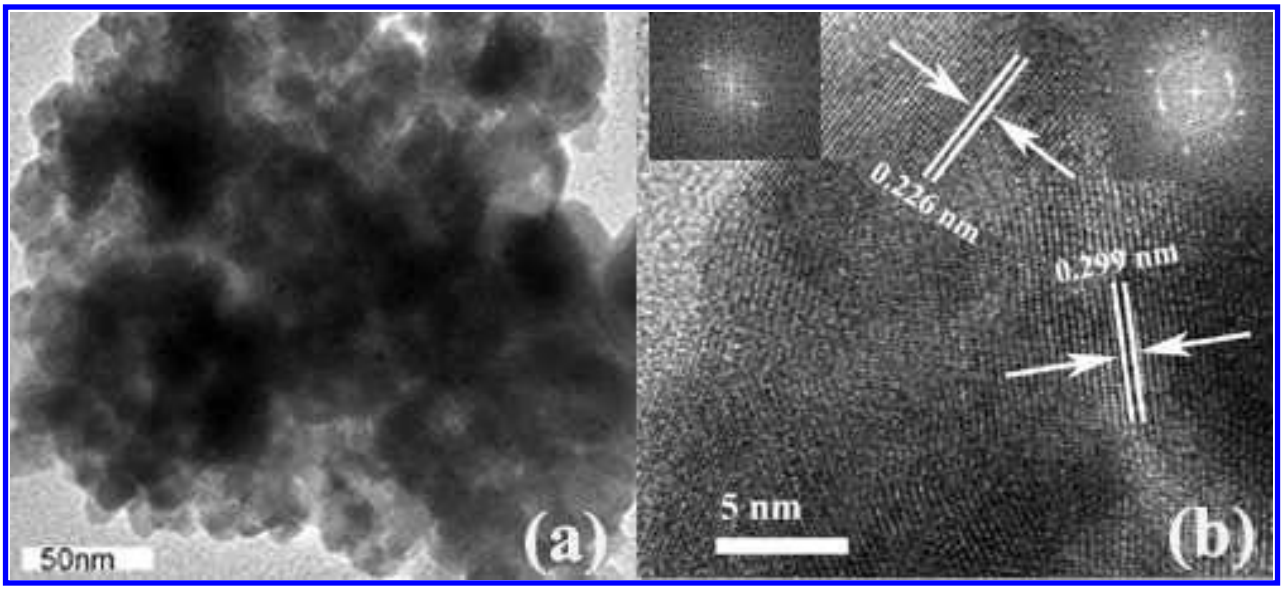

Figure 3. HRTEM imagine of $BiVO_4$–B, the inset in (b) shows the corresponding Fast Fourier transform (FFT) patterns.

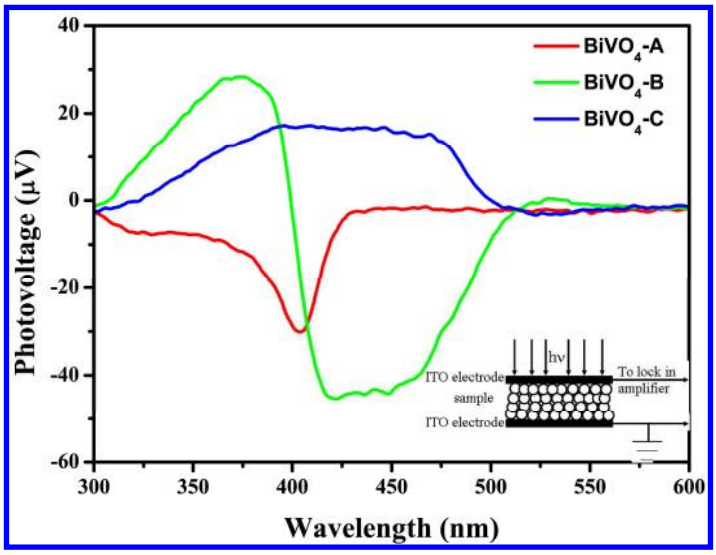

Figure 4. The surface photovoltage spectra (SPS) of samples $BiVO_4$–A, $BiVO_4$–B and $BiVO_4$ –C. Inset is schematic diagram of SPV measurement.

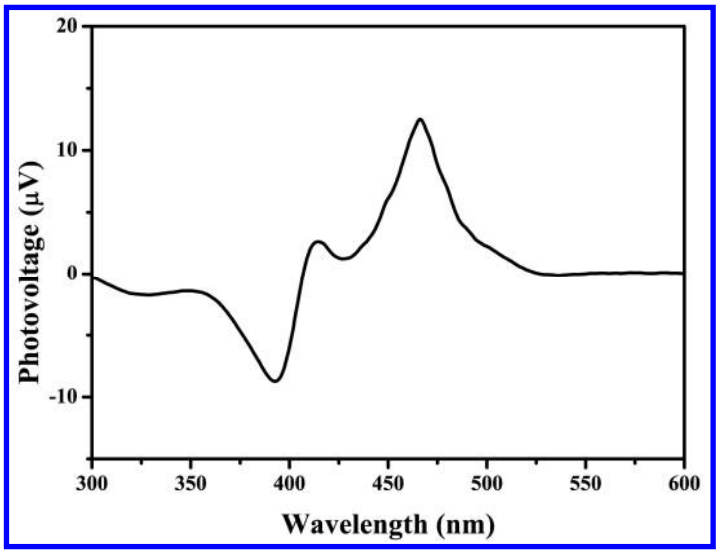

Figure 5. The SPS of direct mixture with the $BiVO_4$–C/$BiVO_4$–A mass ratio of 25.34 %.

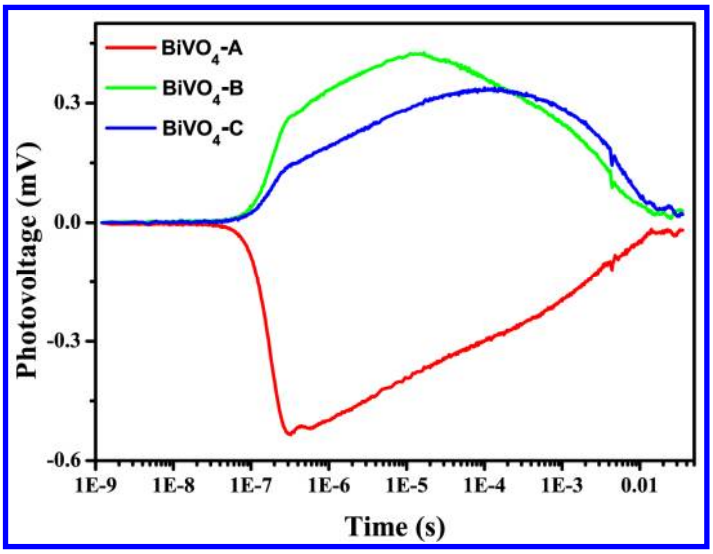

Figure 6. The transient photovoltage (TPV) response of $BiVO_4$. The wavelength and intensity of excitation pulse are 355 nm and 50 μJ, respectively.

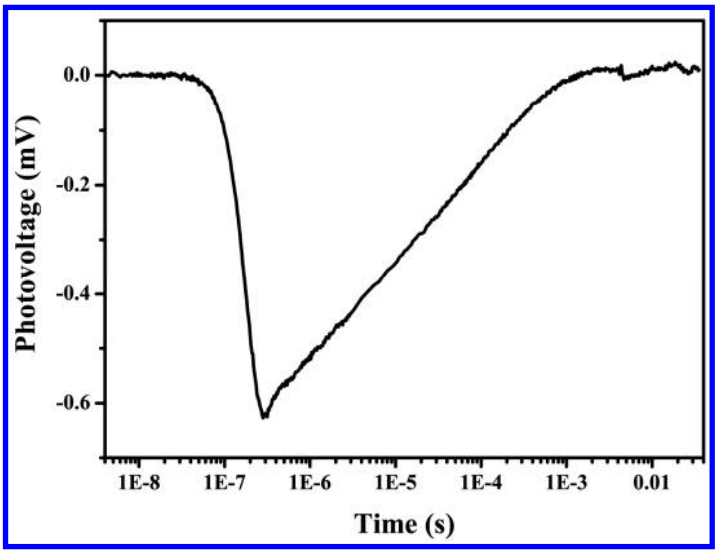

Figure 7. The transient photovoltage (TPV) response of direct mixture with the $BiVO_4$–C/$BiVO_4$–A mass ratio of 25.34 %. The wavelength and intensity of excitation pulse are 355 nm and 50 μJ, respectively.

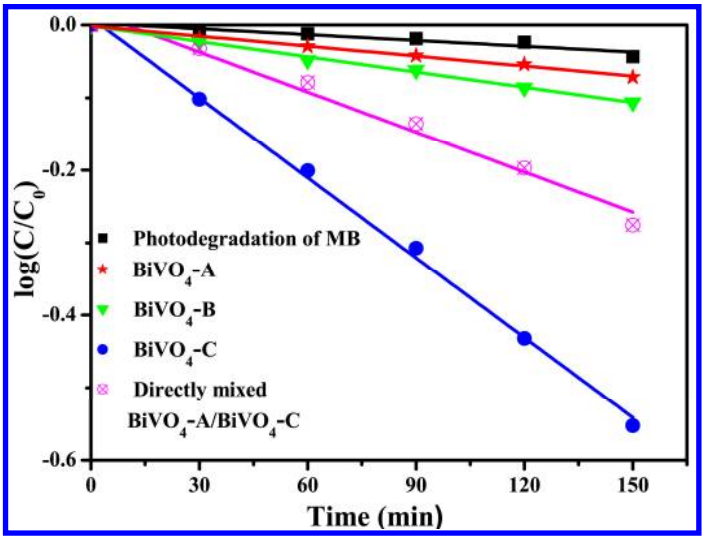

Figure 8. Kinetics of photodegradation of MB using $BiVO_4$ with different crystalline phases under the irradiation of visible light ($\lambda > 400$ nm $C_{MB} = 10$ mg/L).

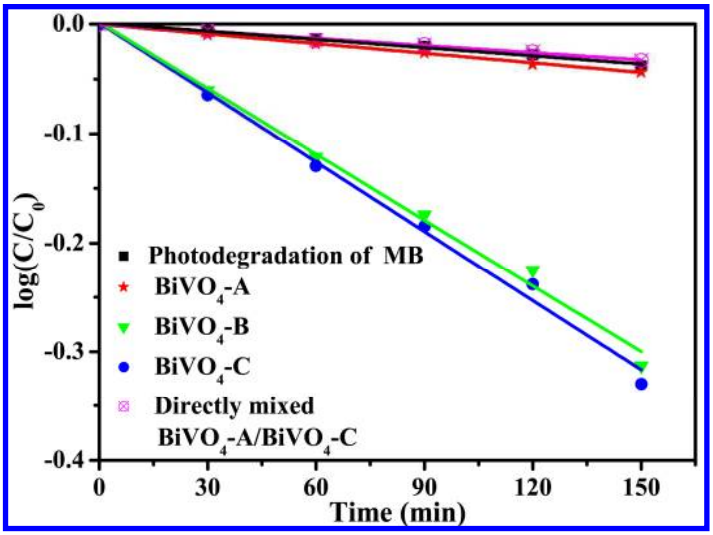

Figure 9. Kinetics of photodegradation of MB using $BiVO_4$ with different crystalline phases under the irradiation of UV light (C_{MB} = 10 mg/L).

Table of Contents (TOC) Image

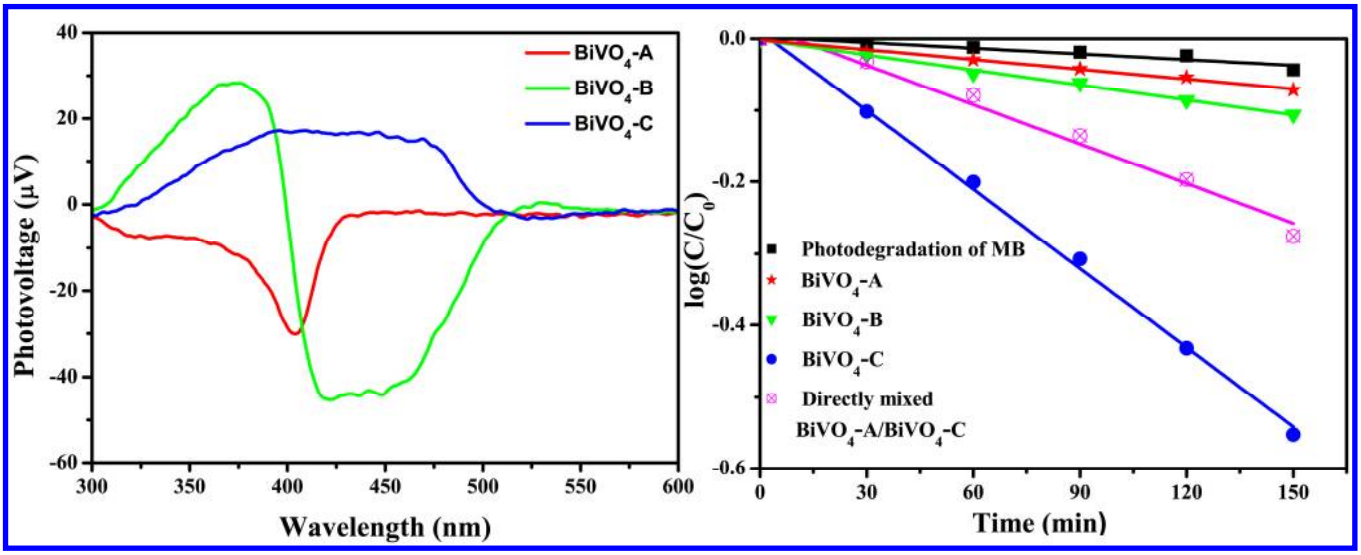

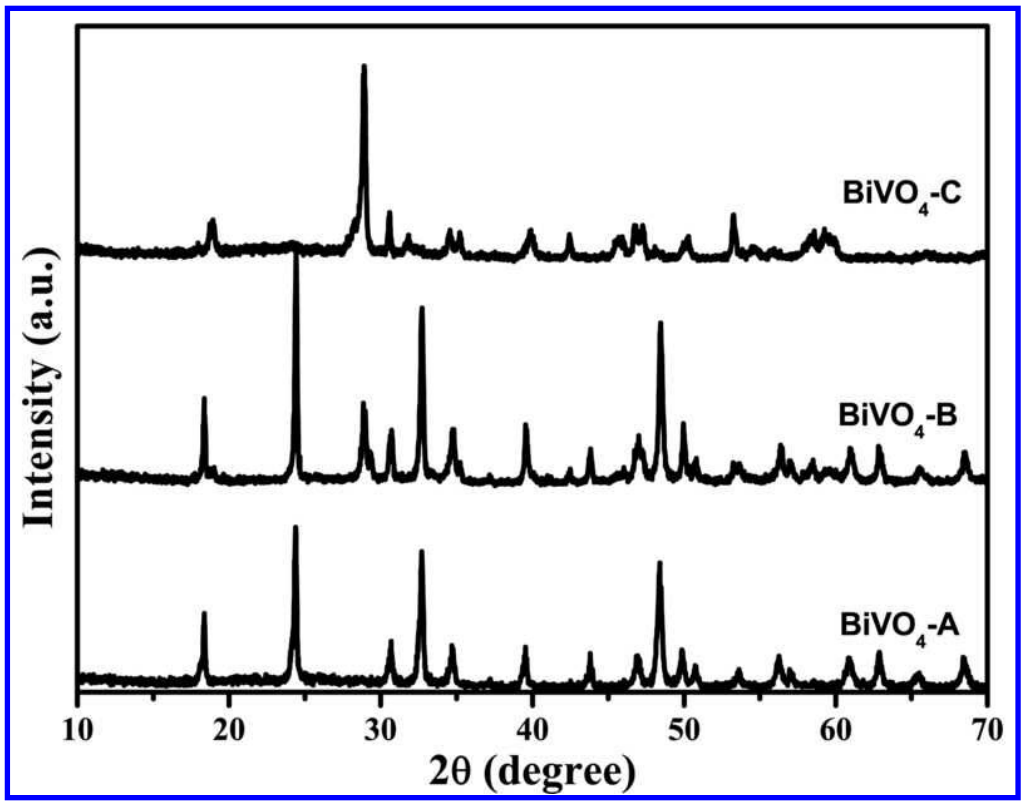

67x52mm (300 x 300 DPI)

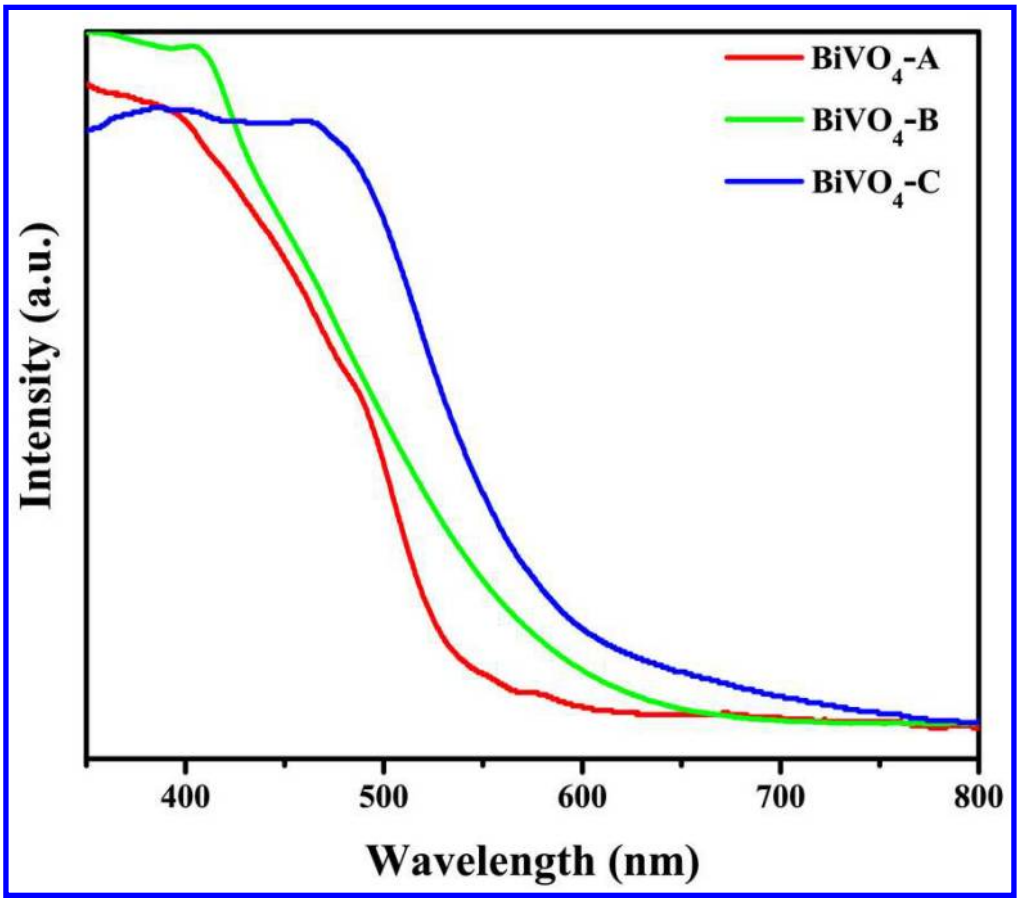

75x66mm (300 x 300 DPI)

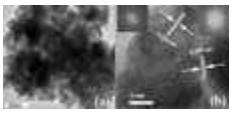

9x4mm (300 x 300 DPI)

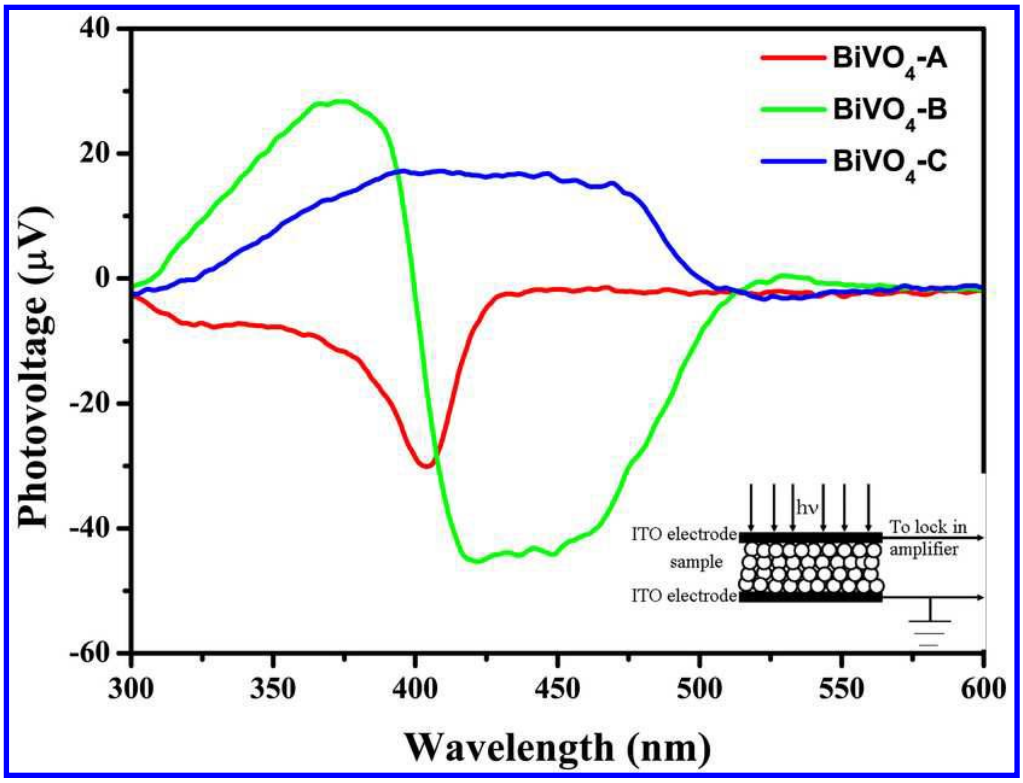

70x53mm (300 x 300 DPI)

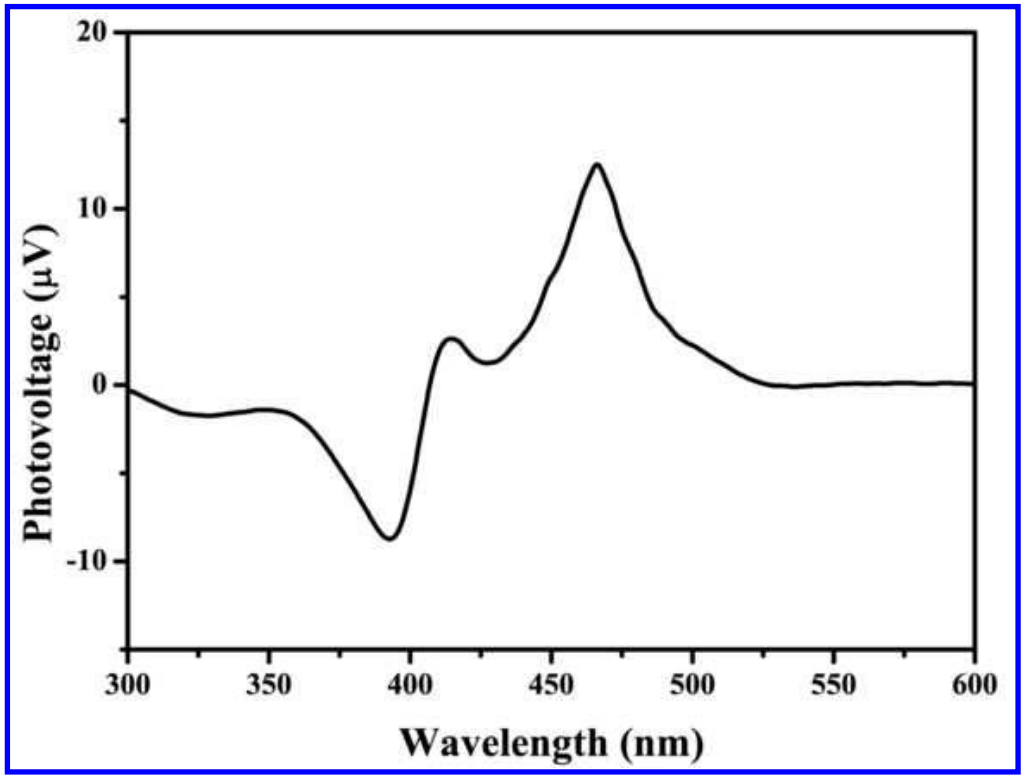

49x37mm (300 x 300 DPI)

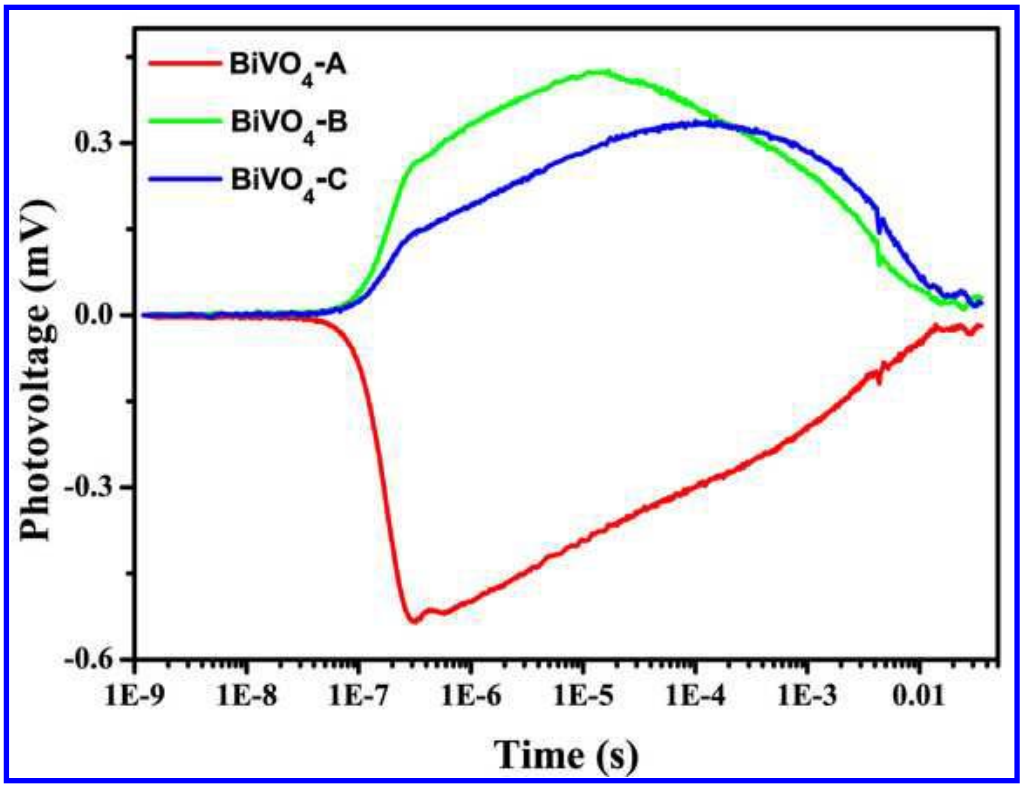

48x37mm (300 x 300 DPI)

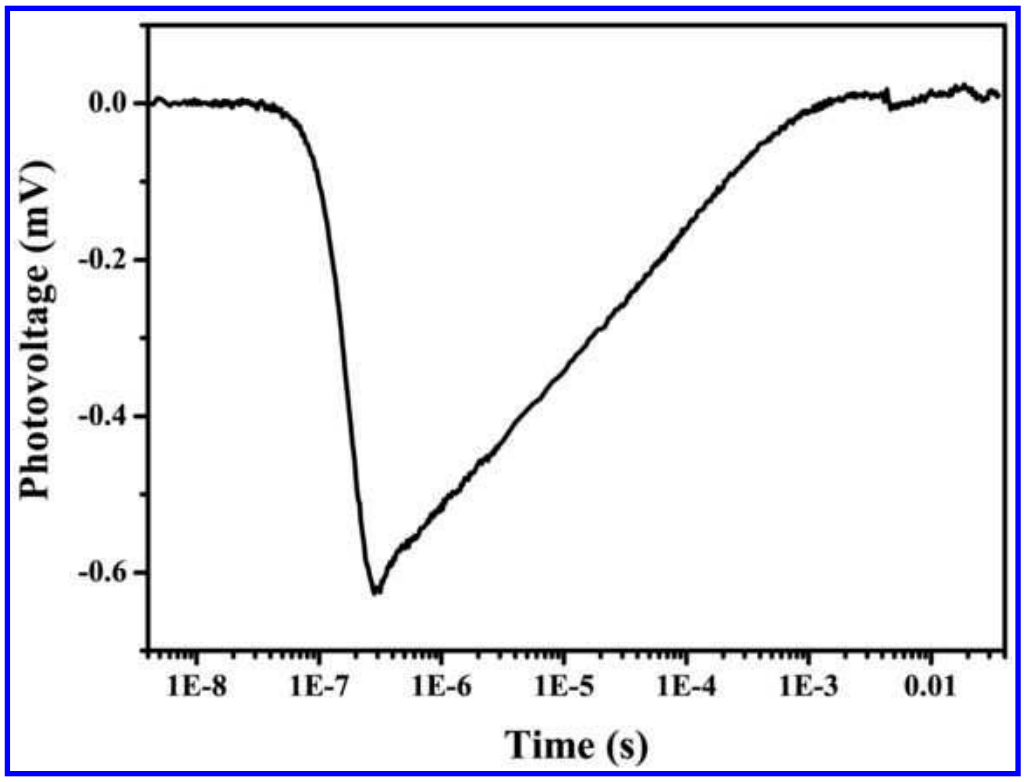

48x36mm (300 x 300 DPI)

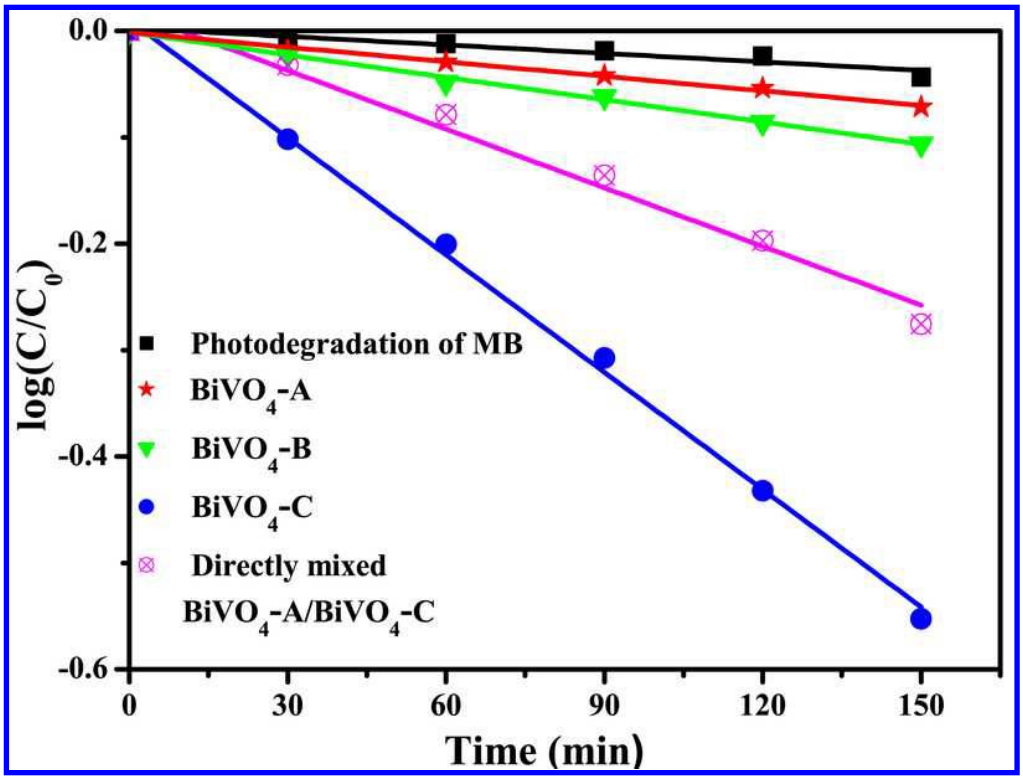

68x51mm (300 x 300 DPI)

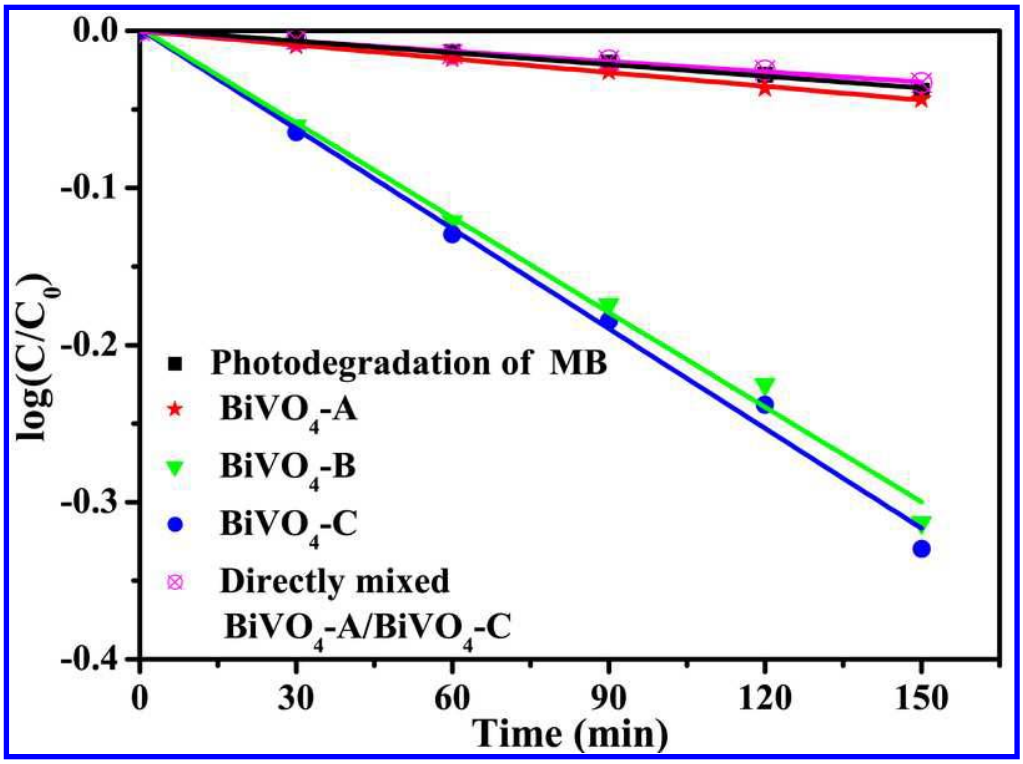

67x50mm (300 x 300 DPI)

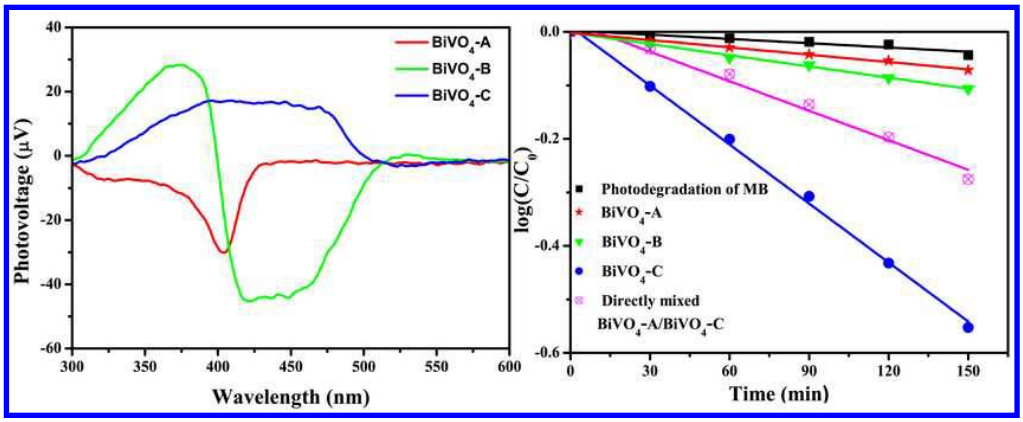

71x28mm (300 x 300 DPI)